Destabilization of barotropic flows by small-scale topography

By E. S. BENILOV[1], J. NYCANDER[2] AND D. G. DRITSCHEL[3]

[1]Department of Mathematics, University of Limerick, Ireland

[2]Department of Meteorology, Stockholm University, Sweden

[3]School of Mathematics, University of St Andrews, UK

The stability of a barotropic zonal jet aligned with zonal topography on the beta-plane is investigated. The topography is assumed to be spatially periodic, with a period much smaller than the width of the jet. The problem is examined both by linear normal-mode analysis and by direct numerical simulations.

The following results are obtained. If the topography is sufficiently weak, the growth-rate of the most unstable normal mode has two maxima. The long-wave maximum occurs at wavelengths comparable to the width of the jet, and is described by Benilov's (*J. Phys. Oceanogr.* vol. 30, 2000, p. 733) asymptotic theory. The short-wave maximum occurs at wavelengths comparable to the scale of the topography or at a shorter one. The nonlinear evolution of the flow is, in this case, similar to that in the case of a flat bottom, i.e. the jet begins to meander and breaks up into separate vortices.

For a stronger topography, long-wave disturbances are stable, as predicted by Benilov's (2000) asymptotic theory, whereas short-wave instabilities are still present. The instabilities are strongest near the lines of maximum shear. In nonlinear simulations, the flow becomes turbulent within narrow strips along these lines, and potential vorticity there homogenizes. As the strips grow wider, they begin to interact, and the subsequent evolution is again similar to that of a jet over a flat bottom: large-scale meandering and break-up of the jet into vortices. In the presence of topography, however, the vortices are 'filled' with short-wave turbulence, and break-up occurs later.

1. Introduction

Most large-scale oceanic currents are unstable, and, in most places, the bottom of the ocean is uneven. Yet, little is known about the effect of bottom topography on the stability of oceanic currents.

In the simplest case of zonal barotropic flow and zonal topography, the monotonicity of potential vorticity (PV) across the flow guarantees stability. Accordingly, the stability of a flow can be affected by topography through its contribution to the PV field: for example, topography can make an otherwise monotonic PV non-monotonic and, thereby, potentially unstable. Note, however, that non-monotonicity of PV is a necessary, but not a sufficient condition for instability.

Pedlosky (1980) considered a problem where topography-induced non-monotonicity of PV does destabilize a three-dimensional quasi-geostrophic flow. In that example, the velocity profile was linear (in both depth and the transverse horizontal variable) and the topography was parabolic, whereas the instability was bottom trapped. Further

examples of destabilization of shear flows by ridges and trenches, both for barotropic flow and for stratified flow, were considered by Schmidt & Johnson (1997).

Benilov (2000a) studied the effect of topography with a much smaller horizontal scale than the flow. He found that such short-scale bottom irregularities can stabilize the traditional jet instability – despite the fact that they make the PV field strongly non-monotonic. Benilov's (2000a) study, however, was not complete, as only long disturbances were considered, with wavelengths comparable to the width of the jet. Short disturbances, with wavelengths comparable to the topographic scale, were not tractable by the asymptotic method employed.

The present paper deals with the stability of large-scale currents over small-scale topography with respect to small-scale disturbances, and thus complements Benilov's (2000a) study. It is organized as follows. In §2, we formulate the governing equations. In §3, we discuss the stability of a uniform shear flow over a single rectangular ridge (this simple example illustrates how topography can destabilize a shear flow). Then, the stability of a Gaussian jet over sinusoidal topography is examined in §4 by means of linear stability analysis and, in §5, by direct simulation of the nonlinear governing equations.

2. Formulation

Consider a barotropic ocean of variable depth $H(x, y)$, where x and y are the spatial coordinates (the x-axis is directed eastwards), on the beta-plane. The flow is described by the streamfunction $\Psi(t, x, y)$, where t is the time. We assume Ψ to be governed by the barotropic vorticity equation (e.g. Pedlosky 1987),

$$\frac{\partial \nabla^2 \Psi}{\partial t} + J(\Psi, \nabla^2 \Psi + D) + \beta \frac{\partial \Psi}{\partial x} = 0, \tag{2.1}$$

where the function

$$D(x, y) = \frac{f_0}{H_0}(H_0 - H)$$

describes the height of topography relative to the mean level of the ocean's bottom (H_0 is the mean depth), f_0 and β are the Coriolis parameter and its meridional gradient, and J is the Jacobian. Equation (2.1) is valid in the quasi-geostrophic limit, i.e. if the Rossby number is small and the topography is weak (i.e. $|H - H_0| \ll H_0$).

In this paper, we consider the simplest case of a zonal flow, $U = U(y)$, aligned with zonal topography, $D = D(y)$. Let the flow be perturbed by a small disturbance, ψ,

$$\Psi = -\int U \, dy + \psi. \tag{2.2}$$

Substitute (2.2) into (2.1) and omit nonlinear terms. For normal modes, i.e. solutions of the form

$$\psi(x, y, t) = \phi(y) e^{i(kx - \omega t)}, \tag{2.3}$$

where k and ω are the wavenumber and frequency of the disturbance, the resulting equation becomes

$$(U - c)\left(\frac{d^2\phi}{dy^2} - k^2\phi\right) + \left(\frac{dD}{dy} + \beta - \frac{d^2U}{dy^2}\right)\phi = 0, \tag{2.4}$$

where $c = \omega/k$ is the phase speed of the disturbance. The boundary conditions are

$$\phi \to 0 \qquad \text{as } y \to \pm\infty. \tag{2.5}$$

(2.4)–(2.5) form an eigenvalue problem, for which ϕ is the eigenfunction and c is the eigenvalue. If Im $c > 0$, the flow is unstable.

Following Fjørtoft's (1950) stability criterion, we can prove that problem (2.4)–(2.5) does not have unstable solutions if there exists a constant C, such that

$$(U - C)\frac{\mathrm{d}Q}{\mathrm{d}y} < 0 \qquad \text{for all } y, \tag{2.6}$$

where $Q(y) = -U'(y) + D + \beta y$ is the potential vorticity of the background flow.

3. Stability of shear flows along a rectangular ridge

In this section, we shall discuss the stability of a uniform shear flow along a rectangular ridge or trench – which is the simplest example illustrating how topography may destabilize an otherwise stable flow. It is also relevant to flows of arbitrary profile, provided the ridge is much narrower than the length scale of the flow.

Consider a 'top hat' topography defined by

$$D(y) = \begin{cases} \dfrac{f_0 \, \Delta H}{H_0} & \text{at } |y| \leqslant \tfrac{1}{2}a, \\ 0 & \text{at } |y| > \tfrac{1}{2}a, \end{cases} \tag{3.1}$$

where a is the width and ΔH the height of the ridge (for a trench, $\Delta H < 0$). Assuming that the wavelength of the disturbance and a are much smaller than the horizontal scale of the flow, we approximate the flow profile locally by a uniformly sheared current,

$$U(y) = Sy,$$

where $S = \mathrm{d}U/\mathrm{d}y$ is the local shear. We also assume that the topography is much stronger than the beta-effect, and therefore neglect the latter. The solution of (2.4) in the three regions defined by (3.1) is then a superposition of simple exponentials, which have to be matched by the appropriate jump conditions at the topographic discontinuities. The calculations are elementary, and the result can also be obtained as a special case of equation (4.6) in Schmidt & Johnson (1997). The resulting dispersion relation is

$$\omega = \pm \tfrac{1}{2}|S|\sqrt{(ka - B)^2 - B^2 \mathrm{e}^{-2ka}}, \tag{3.2}$$

where the *topography amplitude parameter*

$$B = -\frac{f_0 \, \Delta H}{S \, H_0} \tag{3.3}$$

reflects the strength of topography relative to the shear of the flow†.

If ΔH and S are of the same sign (i.e. $B < 0$), we can readily see that ω is real; hence, the flow is stable. If ΔH and S are of opposite signs ($B > 0$), there is a band of unstable wavenumbers (see figure 1). For $B \to \infty$, the unstable band moves towards the short-wave end of the spectrum (it is centred at $k \approx B/a$) and becomes exponentially narrow, whereas the growth rate becomes exponentially small (proportional to e^{-B}). For $B \in (0, 1)$, on the other hand, the band includes $k = 0$, as can be seen by expanding

† Equation (3.2) is the same as obtained previously by Dritschel (1989) for a strip of uniform PV in background shear, if we identify SB with ω, the strip PV, and B with $(1 - \Lambda)^{-1}$, where Λ is the shear to PV ratio. The nonlinear development of unstable strips is discussed in this reference.
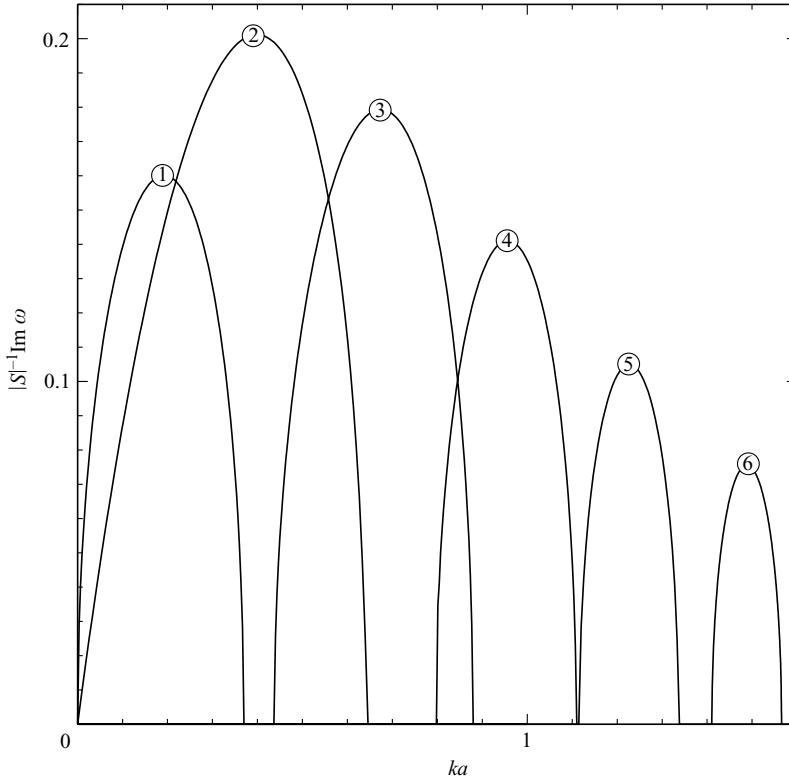
FIGURE 1. The non-dimensional growth rate (3.2) *vs.* non-dimensional wavenumber, for the case of uniformly sheared flow and an isolated rectangular ridge. The topography amplitude parameter (3.3) is $B = 0.5, \ 1, \ 1.5, \ 2, \ 2.5, \ 3$ (curves 1–6, respectively).

equation (3.2) for $ka \ll 1$:

$$\omega \simeq \pm \mathrm{i} |S| \sqrt{\tfrac{1}{2} ka (B - B^2)}.$$

Such large-scale instabilities usually lead to meandering and, physically, are the most important ones.

We conclude, as did Schmidt & Johnson (1997), that a rectangular ridge ($\Delta H > 0$) destabilizes a cyclonic shear flow ($S < 0$), whereas a trench ($\Delta H < 0$) destabilizes an anticyclonic one ($S > 0$). In other words, the flow in this example is unstable in all cases where Fjørtoft's criterion (2.6) does not guarantee stability. Most importantly, the instability has the same length scale as the topography, or even a shorter one (if $B \gg 1$).

For a wide jet over small-scale topography with both ridges and trenches, these results would indicate that short-wave topographic instability occurs on both (cyclonic and anticyclonic) flanks of the jet. However, topographic irregularities are usually not isolated or separated by wide gaps, and disturbances localized near neighbouring irregularities interact with one another. In addition, the sharp edges make a rectangular ridge a poor approximation of real oceanic topography. Thus, in the next section, we shall consider *sinusoidal* topography, which is free from both of these shortcomings.

4. Stability of a Gaussian jet over sinusoidal topography

The stability of barotropic jets over short-scale zonal topography of general shape has previously been examined by Benilov (2000*a*). He showed that modes with a much larger length scale than the topography are stable provided a 'topographic Richardson number' exceeds 1/4,

$$Ri_{topo} = \left(\frac{f_0 \, \overline{\Delta H}}{S_{max} \, H_0} \right)^2 > \tfrac{1}{4},$$

where $\overline{\Delta H}$ is the mean-square height of topography and S_{max} is the maximum shear of the jet. Applying this to sinusoidal topography (for which $\overline{\Delta H} = \Delta H / \sqrt{2}$) yields the stability criterion

$$Ri_{topo} = \tfrac{1}{2} \left(\frac{f_0 \, \Delta H}{S_{max} \, H_0} \right)^2 > \tfrac{1}{4}. \tag{4.1}$$

(Note that $Ri_{topo} = B^2 / 2$ – compare (4.1) with (3.3).)

On the other hand, the simple example discussed in §3 of the present paper indicates that we can expect instabilities for any values of Ri_{topo} at crests or troughs where $B > 0$. The length scale of these unstable modes must be too small for Benilov's (2000*a*) analysis to be applicable. We shall therefore re-examine the problem for a wider range of wavelengths numerically (using a method employed previously by Benilov & Sakov 1999).

Thus, we shall investigate the stability of a Gaussian jet over sinusoidal topography,

$$U(y) = U_{max} \exp \left(- \frac{y^2}{2L^2} \right), \tag{4.2}$$

$$D(y) = \frac{f_0 \Delta H}{H_0} \sin \left(\frac{2\pi y}{a} \right), \tag{4.3}$$

where U_{max} and L are the amplitude and half-width of the jet, and ΔH and a are the amplitude and spatial scale of the topography. We shall consider a strong (in terms of net mass flux) westward current with the parameters

$$U_{max} = -0.25 \, \text{m s}^{-1}, \qquad L = 50 \, \text{km}, \tag{4.4}$$

in a mid-latitude ocean

$$H_0 = 5000 \, \text{m}, \qquad \theta = 30 \text{U}, \tag{4.5}$$

where θ is the latitude. Note that, for disturbances with a length scale comparable to that of the jet, the beta-effect is relatively weak, but not negligible – as characterized by the following non-dimensional parameter:

$$\frac{\beta L^2}{U_{max}} \approx 0.2.$$

However, for disturbances with a similar length scale to the topography, the beta-effect can be neglected. The parameters of the topography were chosen on a more or less *ad hoc* basis. We assume that the distance between two neighbouring topographic crests is a tenth of the half-width of the jet,

$$a = 5 \, \text{km}, \tag{4.6}$$

and consider several particular values of ΔH in the range

$$0 \leqslant \Delta H \leqslant 150 \, \text{m}. \tag{4.7}$$
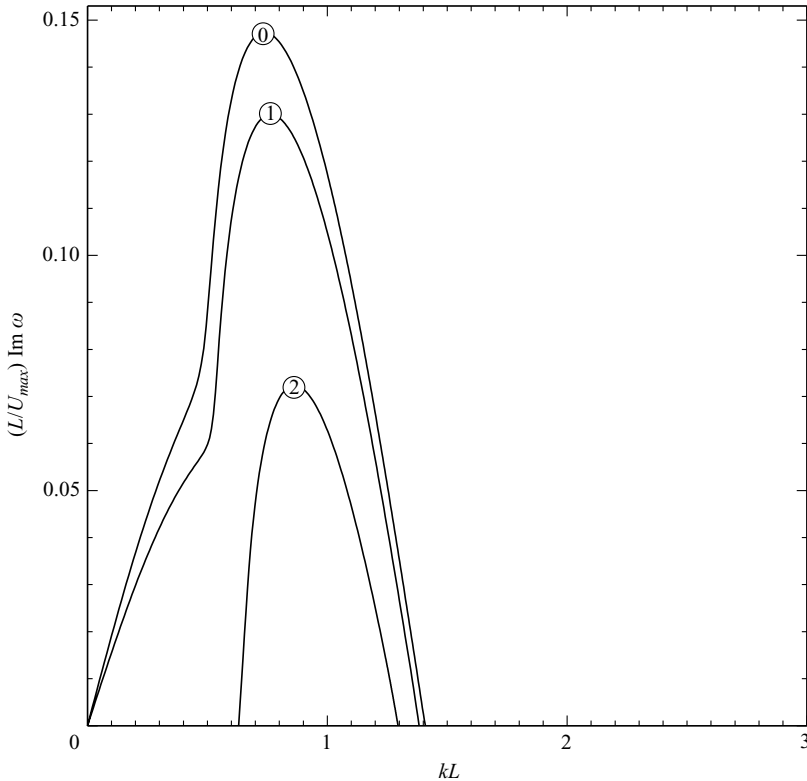
FIGURE 2. The asymptotic (Benilov 2000*a*) non-dimensional growth rate *vs.* non-dimensional wavenumber, for the Gaussian jet and sinusoidal topography (4.2)–(4.6). The height of topography is $\Delta H = 0, 50, 100$ (curves 0–2, respectively).

First of all, we examine (4.2)–(4.7) using Benilov's (2000*a*) asymptotic theory. Only one mode is found, and it is unstable for $\Delta H \lesssim 145$ m. (Its growth rate for various values of ΔH is shown in figure 2.) At $\Delta H \approx 145$ m, topography stabilizes the flow. In this case, $Ri_{topo} \approx 0.242$, so that criterion (4.1) is almost satisfied.

The growth rate of the same mode (which will be referred to as the 'main' mode) has also been computed using the exact equation (2.4). A typical case ($\Delta H = 50$ m) is illustrated in figure 3. The following features of the main mode can be observed:

(i) For $kL \lesssim 1$, the asymptotic curve is indistinguishable from the exact one, but, for shorter wavelengths, the two curves diverge (figure 3). Most importantly, instability exists far beyond $kL \approx 1.38$, where the asymptotic theory places its short-wave cutoff.

(ii) For $kL \gtrsim 3$, the eigenfunction has two localization points, $y = \pm y_*$, which are situated at the topographic crest or trough closest to the point of maximum shear. The disturbance is no longer sensitive to the global structure of the jet, and these localization points can be examined separately. Furthermore, the jet profile (4.2) can now be replaced by its expansion about y_*,

$$U \approx U_{max} \exp\left(-\frac{y_*^2}{2L^2}\right) \left[1 - \frac{y_*}{L^2}(y - y_*)\right], \tag{4.8}$$

or a similar expansion about $-y_*$ (both cases result in the same growth rate). In addition, since we are dealing with short disturbances, we can neglect the beta-effect,
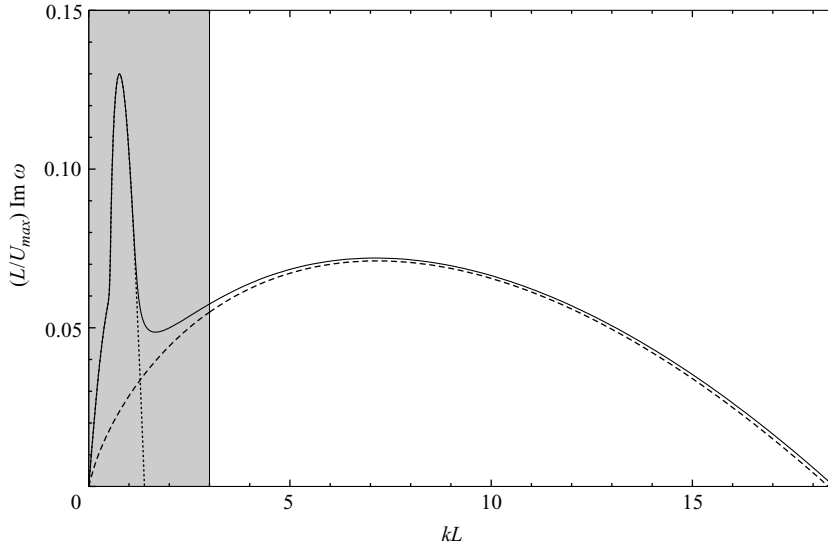
$$\beta = 0. \tag{4.9}$$

FIGURE 3. The non-dimensional growth rate *vs.* non-dimensional wavenumber, for the Gaussian jet and sinusoidal topography, (4.2)–(4.6), with $\Delta H = 50\,\text{m}$ ($B = 0.24$, $Ri_{topo} = 0.029$). The solid line shows the numeric solution of the exact equation (2.4), the dotted line shows Benilov's (2000a) long-wave approximation, and the dashed line shows the approximation of local shear (4.8)–(4.9). The shaded region in this figure corresponds to the entire area of figure 2.

In what follows, approximation (4.8)–(4.9) will be referred to as the 'approximation of local shear' (ALS). The growth rate when using ALS is shown in figure 3 – we can see that it approximates the exact growth rate sufficiently well.

Unlike the asymptotic model, the exact equation (2.4) has more than one eigenmode, and the most convenient way to classify them is to consider a sufficiently large k, in which case the eigenfunctions become localized near topographic crests or troughs. Modes localized closer to the point of maximum shear have higher growth rates, with the 'closest' mode being, generally, the most unstable one.

We have examined other examples, two of which ($\Delta H = 100\,\text{m}$ and $\Delta H = 150\,\text{m}$) are shown in figures 4a and 4b. In the latter case, topography is strong enough to completely eliminate the long-wave maximum of the growth rate. Note that the necessity of resolving the long scale L associated with the jet and the short topographic scale a makes the exact equation (2.4) extremely difficult to solve numerically. The difficulty becomes particularly severe for larger ΔH and k – as a result, we were unable to solve (2.4) with a consistently high accuracy for $\Delta H > 50\,\text{m}$, $kL > 3$. Instead, we used the approximation of local shear (the uniform shear flow (4.8) does not have an intrinsic spatial scale, hence, a is the only spatial scale – which makes this problem easy to solve numerically). For growing ΔH, the ALS works increasingly well, which is particularly visible in figure 4b.

We have also calculated the dimensional parameters of the long- and short-wave maxima of the growth rate, for various heights of topography (see table 1).

The following conclusions can be drawn from figure 4 and table 1:

(i) As the height of topography grows, the asymptotic approach fails completely, and for $\Delta H \geqslant 145\,\text{m}$ (for which $Ri_{topo} > 1/4$, and criterion (4.1) predicts stability) the flow is still unstable.
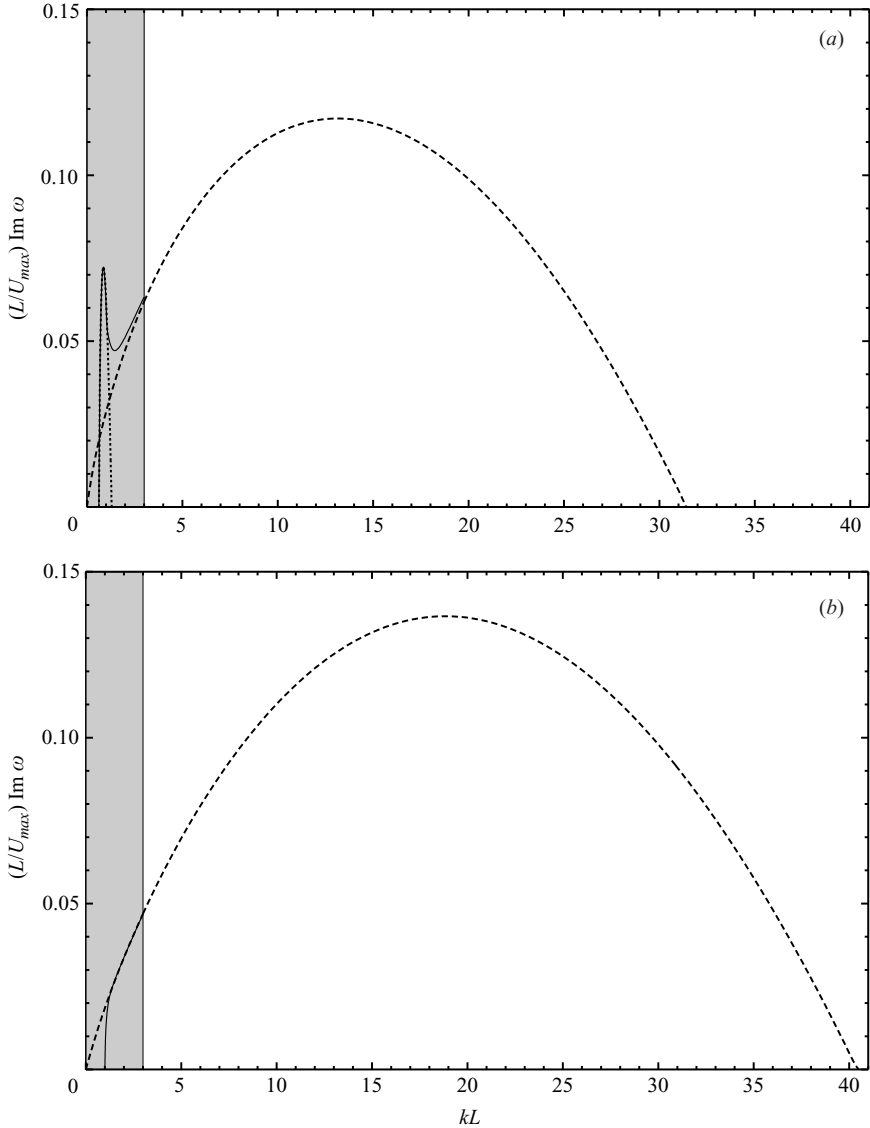
FIGURE 4. The same as figure 3, but for: (a) $\Delta H = 100$ m ($B = 0.48$, $Ri_{topo} = 0.114$); (b) $\Delta H = 150$ m ($B = 0.72$, $Ri_{topo} = 0.258$). The long-wave stability criterion (4.1) is satisfied; hence, the asymptotic growth rate is zero and is not shown.

	$\Delta H = 0$ m	$\Delta H = 50$ m	$\Delta H = 100$ m	$\Delta H = 150$ m
LWM	$\lambda \approx 214$ km $\tau \approx 12$ days	$\lambda \approx 207$ km $\tau \approx 18$ days	$\lambda \approx 182$ km $\tau \approx 32$ days	—
SWM	—	$\lambda \approx 22$ km $\tau \approx 32$ days	$\lambda \approx 12$ km $\tau \approx 20$ days	$\lambda \approx 8$ km $\tau \approx 17$ days

TABLE 1. The dimensional parameters of the long- and short-wave maxima (LWM and SWM) of the growth rate, for various heights of topography. $\lambda = \pi k^{-1}$ is the spatial scale, $\tau = (\mathrm{Im}\,\omega)^{-1}$ is the e-folding time.

(ii) Ineasing topography moves the instability toward the short-wave end of the spectrum. (The most unstable wavenumber is approximately proportional to the height of topography, as suggested by the scaling $k \approx B/a$ obtained for the rectangular ridge.) It also gradually strengthens the instability†.

In addition to the strong westward jet (4.4) illustrated here, we have also examined westward and eastward jets with other parameters. Similar results have been obtained, with one exception: the beta-effect influences eastward currents more strongly than their westward counterparts and, as a result, eastward jets are less susceptible to long-wave instability. The short-wave instability, in turn, is not sensitive to the beta-effect and all our conclusions remain exactly the same.

The short-wave topographic modes are by themselves unable to cause meandering and break up the jet. Does this mean that they are unimportant physically? This question cannot be answered by the normal-mode stability analysis; it will be addressed in the next section by direct numerical simulations.

5. Simulations of a Gaussian jet over sinusoidal topography

In order to investigate the long-term evolution of the jet, (2.1) has been simulated numerically by means of the CASL algorithm (Dritschel & Ambaum 1997, see also the Appendix). We have simulated the Gaussian jet, (4.2), with parameters (4.4)–(4.5), for a wide range of topographies ((4.3), (4.6) with $0 \leqslant \Delta H \leqslant 500\,\text{m}$). The computational domain is a periodic channel of length and width $2L_c$, with free-slip rigid-wall boundary conditions in y:

$$\frac{\partial \Psi}{\partial x} = 0 \qquad \text{at } y = \pm L_c.$$

The half-width of the channel used in the simulations is approximately $L_c = 160\,\text{km}$, which is a little more than three times wider than the jet. Such a relatively narrow channel can be used because of the short-wave nature of the instabilities (which are mainly localized in the jet and do not spread out). At the same time, large-scale flows over short-scale topography are extremely difficult to model numerically, and we needed all the resolution we could muster.

The initial condition consists of a weakly perturbed Gaussian jet, as described in the Appendix. Several examples of topography have been examined, with the following results.

If the topography is weak ($\Delta H < 150\,\text{m}$) and does not stabilize long-wave disturbances, the evolution of the flow is similar to that in the case of a flat bottom – i.e. the jet begins to meander and breaks up into separate vortices (see figure 5). Unlike the flat bottom case, however, these vortices are 'filled' with short-wave turbulence.

If the topography is strong enough to suppress the long-wave instability, the short-wave instability first develops in accordance with the linear analysis presented in the previous section. An example with $\Delta H = 150\,\text{m}$ can be seen in figure 6. Instability first appears near the lines of maximum shear, where the growth rate is largest (its wavenumber differs from the wavenumber of maximum growth, computed through linear normal-mode theory, by no more than 3%). The growing disturbances then become nonlinear and 'roll up' (at $t \sim 90\,\text{days}$). Eventually, two turbulent strips form (at $t \sim 110\,\text{days}$), the potential vorticity within which has, to a certain extent,

† This conclusion applies to topography with $\Delta H \leqslant 500\,\text{m}$. For larger ΔH, the instability evens out and begins to weaken.
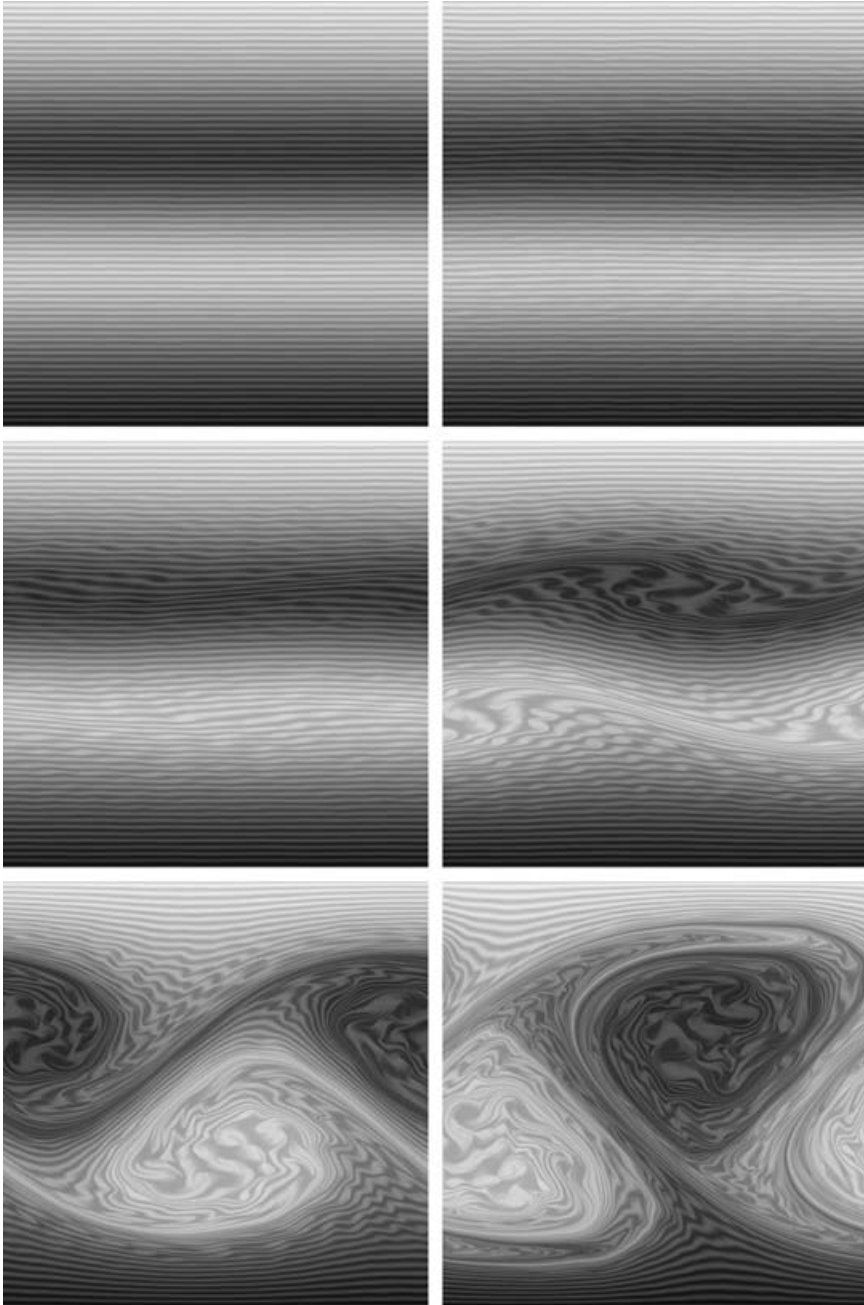
Figure 5. Evolution of PV for a Gaussian jet over sinusoidal topography, (4.2)–(4.6), with $\Delta H = 50$ m. The times shown are $t = 15,\ 51,\ 87,\ 124,\ 160,\ 196$ days.

homogenized (see figure 7a). Effectively, this means that a rapidly varying zonal flow develops in the strips, which cancels the topographic part of the PV, and at the same time has a small enough amplitude to leave the velocity profile essentially unperturbed (see figure 7b). The turbulent strips gradually grow wider, and at $t \approx 160$ days begin to interact, which leads to meandering. This can be interpreted as a secondary instability
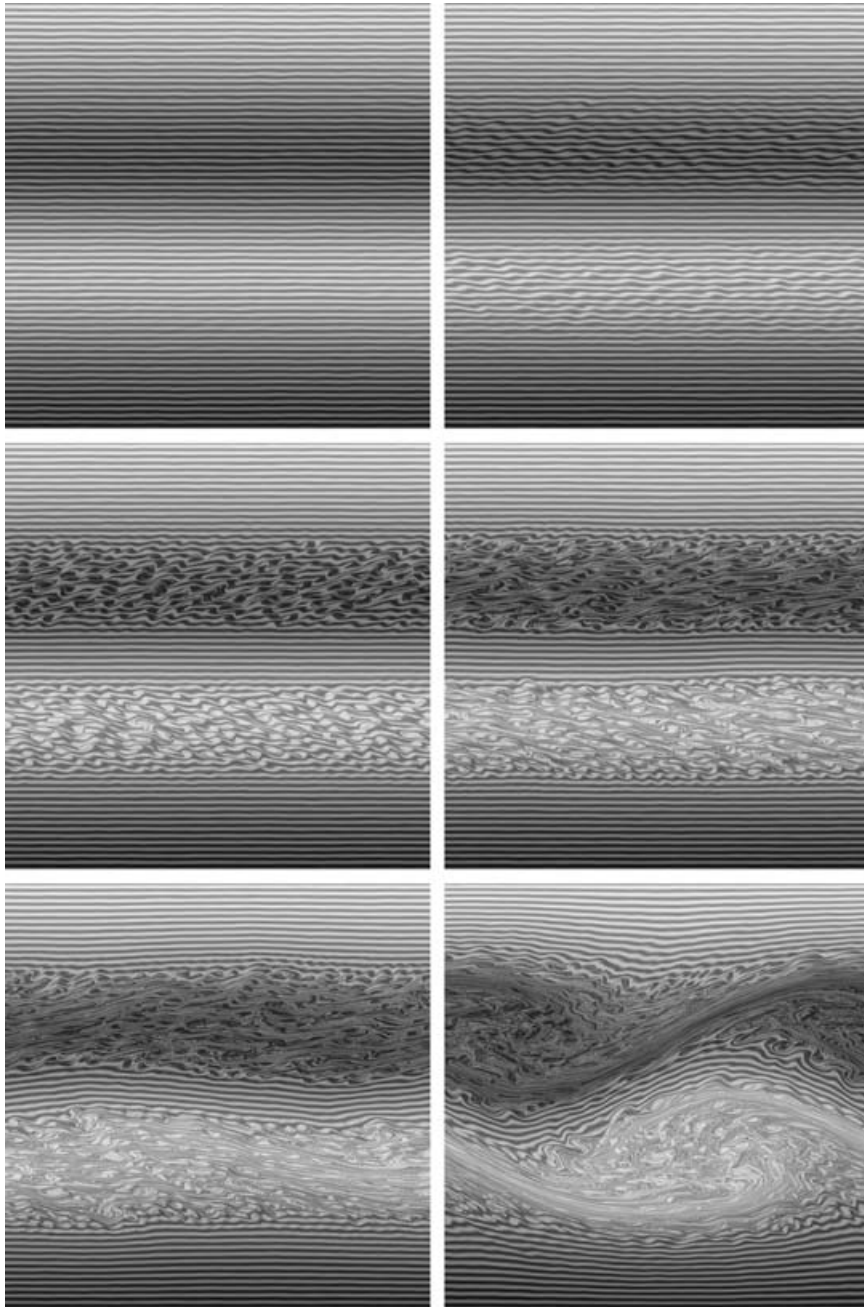
FIGURE 6. Evolution of PV for a Gaussian jet over sinusoidal topography, (4.2)–(4.6), with $\Delta H = 150$ m. The times shown are $t = 15, \ 51, \ 87, \ 124, \ 160, \ 196$ days.

acting on a flow with partially homogenized PV, i.e. the PV-homogenized strips destabilize long-wave disturbances, which were initially stable because of small-scale topography.

Eventually, the jet breaks up into turbulence-filled vortices – see the last frame ($t = 196$ days) of figure 6. Note, however, that the vortices are very weak, and the
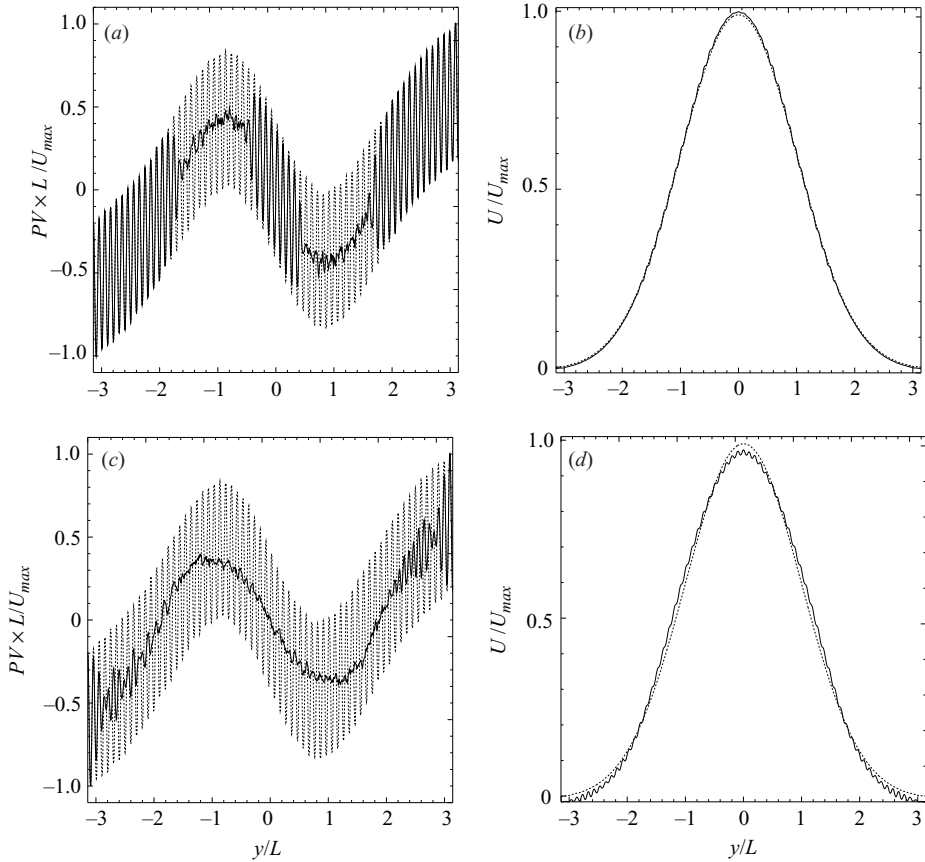
FIGURE 7. Zonally averaged non-dimensional characteristics of the jet with $\Delta H = 150$ km *vs.* non-dimensional y. The initial profiles are shown by dotted lines. (*a*) potential vorticity at $t = 110$ days, (*b*) velocity at $t = 110$ days, (*c*) potential vorticity at $t = 196$ days, (*d*) velocity at $t = 196$ days.

mean flow is essentially intact (it has lost less than 3% of its initial amplitude, see figure 7*d*).

   We have also examined two cases of stronger topography, $\Delta H = 350$, 500 m. It turned out that these are qualitatively similar to the previous case, but turbulent strips with homogenized PV develop later (at the same time, suprisingly, the linear growth rates in the cases considered are very close: the e-folding times for $\Delta H = 150$, 350, 500 m are $\tau = 17$, 17, 18 days, respectively).

6. Summary and concluding remarks

   We have examined the stability of a jet over short-scale sinusoidal topography. A normal-mode linear analysis has been carried out (§4), supported by simulations of the nonlinear flow evolution (§5). The following results have been obtained.

   If the topography is weak and does not satisfy Benilov's (2000*a*) asymptotic stability criterion (4.1), the growth rate has two maxima (a typical example is shown in figure 3). The long-wave maximum occurs at wavelengths comparable to the width of the jet and is described by Benilov's (2000*a*) asymptotic theory. The short-wave maximum is

associated with topography. Many unstable short-wave modes exist, each having two localization points at topographic crests or troughs located on opposite flanks of the jet. The mode with the largest growth rate is localized near the points of maximum shear.

In this case, the nonlinear large-scale evolution of the flow is similar to that in the flat-bottom case, i.e. the jet begins to meander and breaks up into separate vortices (see figure 5). Because of the short-wave topographic modes, the vortices are filled with small-scale turbulence.

For stronger topographies, satisfying criterion (4.1), the linear analysis shows that there is no long-wave instability. The short-wave modes, however, are still present and, in nonlinear simulations, they evolve into turbulent strips centred around the lines of maximum shear on the flanks of the jet. Within these strips, the PV field is homogenized by the turbulence. The perturbation of the zonally averaged flow implied by the homogenization is very small compared to the background flow.

The strips slowly widen and start to interact, which leads to a large-scale secondary instability. Because of this instability, the jet meanders and, eventually, breaks up into vortices. Compared to the case of a flat bottom, however, breakup occurs later and slower.

Note that our results justify applications of Rayleigh's and Fjørtoft's stability criteria to large-scale oceanic flows, even though oceanic topography seems to violate both of these conditions. Indeed, since short-scale topographically induced PV variations give rise to short-wave instability which homogenizes the PV field, we conclude that the most relevant initial condition in modelling geophysical problems includes a weak short-scale flow component that compensates for the short-scale topographic PV variations. The resulting PV field varies on the scale of the flow, rather than on that of the topography.

Note also that such a PV-field does not support topographic waves of the kind studied by Rhines & Bretherton (1973), Reznik & Tsybaneva (1999), Bobrovich & Reznik (1999), Vanneste (2000, 2003), Benilov (2000*a*) and others. In fact, our results call the practical reality of such waves into question, since they require for their existence small-scale PV-variations which are unstable in the presence of a large-scale flow.

Finally, we note that the model used in the present paper must be extended to include density stratification of the ocean and two-dimensional topography. The former is relatively easy to implement (see Samelson 1992; Reznik & Tsybaneva 1999; Bobrovich & Reznik 1999; Benilov 2001; Vanneste 2003). The latter extension is much more difficult: so far, only one setting has been found, where the problem has an analytic solution (Vanneste 2000; Benilov 2000*b*). It appears that numerical simulation is the only tool available for the case of two-dimensional topography.

Appendix. Numerical simulations

A.1. *Basic approach*

The nonlinear flow evolution is simulated using the Contour-Advective Semi-Lagrangian (CASL) algorithm (Dritschel & Ambaum 1997). In this algorithm, PV advection is enforced explicitly by tracking a set of PV contours, across which the PV jumps by an increment Δq. The contours are represented by a finite variable number of points between which local cubic splines are used for interpolation (details for this and other aspects of the algorithm may be found in Dritschel & Ambaum 1997).
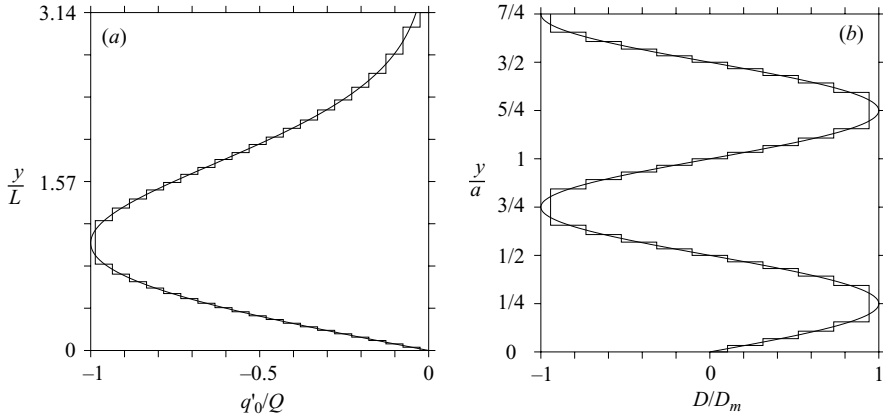
FIGURE 8. The discretization used. (*a*) The discrete profile of q_0'/Q for the Gaussian jet used in the simulations reported, in the domain $[0, \pi]$ in $\pi y/L$ (vertical axis) and $[-1, 0]$ in q_0'/Q (horizontal axis), with 20 PV levels (L is the half-width of the channel, $Q = \max\{q'\}$). (*b*) The discrete profile of the dimensionless topography $D/D_m = \sin 2\pi y/a$, where $D_m = f_0 \Delta H/H_0 q_0'/Q$, in the domain $[0, 7a/4]$ in $\pi y/L$ (vertical axis) and $[-1, 1]$ in D/D_m (horizontal axis). Here, five PV levels are shown, as used in the simulations reported.

The CASL algorithim also makes use of an underlying grid to obtain the velocity field efficiently. This is done by inverting the definition of PV, $q = \nabla^2 \Psi + D + \beta y$, for the streamfunction Ψ and then differentiating Ψ with respect to x and y. Details of this procedure differ little from that discussed in Dritschel & Ambaum (1999) for the three-dimensional (multi-layer) algorithm, apart from the use here of rigid-wall boundaries in y to simulate flow in a periodic channel. Conservation of momentum (in x) is enforced explicitly.

A.2. *PV discretization*

The CASL algorithm works with material contours, here contours of the full PV,

$$q = q' + \beta y + D,$$

where $q' = \nabla^2 \Psi$ is the part of the PV associated with the flow and D is the contribution of topography. Hence, to recover Ψ from q, we invert Laplace's operator on $q - \beta y - D$. Initially, β, D, and the flow $q'(x, y, 0) = q_0'(x, y)$ are all given. From these, we construct the initial PV $q_0 = q_0' + \beta y + D$ by linearly superposing the flow, the background planetary vorticity, and the topography. This is done here by discretizing each effect separately and then superposing the contours.

The planetary vorticity βy is discretized using $n_\beta = 128$ equally-spaced contours, with equal PV jumps $\Delta q_\beta = \beta L_c/n_\beta$, where L_c is the half-width of the channel (see DiBattista & Polvani 1998; Lam & Dritschel 2001).

The discretization of the initial flow q_0' and topography D are accomplished in the same manner. Equal PV jumps are used (or half jumps adjacent to the domain walls) with care to ensure that the circulation contained between any pair of jumps is equal to the corresponding circulation of the continuous distributions of q_0' and D. Figure 8 illustrates the discretization of these profiles used in the current work.

A.3. *The initial disturbance*

In order to introduce a disturbance in the otherwise zonal problem, all of the PV contours are disturbed by randomly displacing each node in y by up to one grid length

(uniformly). Then 10 successive 1-2-1 averagings are done (for each node and the nodes adjacent to it) to smear the disturbance in x, but after each averaging the initial r.m.s. displacement of the contour is restored by multiplying the node displacements by an appropriate factor. This results in a random disturbance correlated over about 10 grid lengths in x and reduces the high-wavenumber component. Pure random noise can lead to local contour slopes of order unity and can cause contour folding before the onset of the linear instability. Averaging keeps the initial contour slopes small, consistent with linear theory.

A.4. *Parameter settings*

In all the simulations conducted, we have ensured an equal grid length in the x and y directions, $\Delta y = \Delta x$. Also, we have used a grid 4 times finer in each direction ($m_g = 4$) to carry out the PV contour-to-grid conversion (before averaging back to the inversion grid, where the velocity is computed). The node distribution and redistribution on contours depends on two prescribed lengths: L, which characterizes the broad features of the PV field, and δ, the smallest contour scale as well as the scale of 'surgery.' In the Gaussian jet simulations, L is chosen to be twice the wavelength of the most unstable linear mode. The surgical scale is given by $\delta = \Delta x/(5m_g)$, or a twentieth of the grid scale (for $m_g = 4$), following the recommended setting in Viúdez & Dritschel (2002). From these two parameters, the dimensionless node-spacing parameter is computed from $\mu = 2\sqrt{\delta/L}$. The density of nodes along a contour is approximately proportional to the square root of curvature and inversely proportional to μ – details may be found in Dritschel & Ambaum (1997). Nodes are redistributed every other time step.

For the time integration, a fourth-order Runge–Kutta method is used with the recommended time step $\Delta t \lesssim 0.025/\max(|q'_{max}|, |D_m|)$. Note that no CFL condition is required for stability.

REFERENCES

BENILOV, E. S. 2000*a* The stability of zonal jets in a rough-bottomed ocean on the barotropic beta-plane. *J. Phys. Oceanogr.* **30**, 733–740.

BENILOV, E. S. 2000*b* Barotropic Rossby waves over two-dimensional topography. *J. Fluid Mech.* **423**, 263–273.

BENILOV, E. S. 2001 Baroclinic instability of two-layer flows over bottom topography. *J. Phys. Oceanogr.* **31**, 2019–2025.

BENILOV, E. S. & SAKOV, P. V. 1999 On the linear approximation of velocity and density profiles in the problem of baroclinic instability. *J. Phys. Oceanogr.* **29**, 1374–1381.

BOBROVICH, A. V., & REZNIK, G. M. 1999 Planetary waves in a stratified ocean of variable depth. Part 2. Continuously stratified ocean. *J. Fluid Mech.* **388**, 147–169.

DIBATTISTA, M. T. & POLVANI, L. M. 1998 Barotropic vortex pairs on a rotating sphere. *J. Fluid Mech.* **358**, 107–133.

DRITSCHEL, D. G. 1989 On the stabilization of a two-dimensional vortex strip by adverse shear. *J. Fluid Mech.* **206**, 193–221.

DRITSCHEL, D. G. & AMBAUM, M. H. P. 1997 A contour-advective semi-Lagrangian numerical algorithm for simulating fine-scale conservative dynamical fields. *Q. J. R. Met. Soc.* **123**, 1097–1130.

FJØRTOFT, R. 1950 Application of integral theorems in deriving criteria of stability for the baroclinic circular vortex. *Geophys. Publ.* **17**, 1–52.

LAM, J. S.-L. & DRITSCHEL, D. G. 2001 On the beta-drift of an initially circular vortex patch. *J. Fluid Mech.* **436**, 107–129.

PEDLOSKY, J. 1980 The destabilization of shear flow by topography. *J. Phys. Oceanogr.* **10**, 1877–1880.

PEDLOSKY, J. 1987 *Geophysical Fluid Dynamics.* Springer.

REZNIK, G. M. & TSYBANEVA, T. B. 1999 Planetary waves in a stratified ocean of variable depth. Part 1. Two-layer model. *J. Fluid Mech.* **388**, 115–145.

RHINES, P. B. & BRETHERTON, F. 1973 Topographic Rossby waves in a rough-bottom ocean. *J. Fluid Mech.* **61**, 583–607.

SAMELSON, R. M. 1992 Surface-intensified Rossby waves over rough topography. *J. Mar. Res.* **50**, 367–384.

SCHMIDT, G. A. & JOHNSON, E. R. 1997 Instability in stratified rotating shear flow along ridges. *J. Mar. Res.* **55**, 915–933.

VANNESTE, J. 2000 Rossby-wave frequency change induced by small-scale topography. *J. Phys. Oceanogr.* **30**, 1820–1826.

VANNESTE, J. 2003 Nonlinear dynamics over rough topography: barotropic and stratified quasi-geostrophic theory. *J. Fluid Mech.* **474**, 299–318.

VIÚDEZ, A. & DRITSCHEL, D. G. 2002 An explicit potential vorticity conserving approach to modelling nonlinear internal gravity waves. *J. Fluid Mech.* **458**, 75–101.